EWS: Exponential Windowing Scheme to Improve LoRa Scalability

Deepak Saluja [ID], Rohit Singh [ID], *Graduate Student Member, IEEE*, Sukriti Gautam, and Suman Kumar

Abstract—**Internet-of-Things (IoT) applications require a network that covers a large geographic area, consumes less power, is low-cost, and is scalable with an increasing number of connected devices. Low-power wide-area networks (LPWANs) have recently received significant attention to meet these requirements of IoT applications. Long-range wide-area network (LoRaWAN) with long range (LoRa) (the physical layer design for LoRaWAN) has emerged as a leading LPWAN solution for IoT. However, LoRa networks suffer from the scalability issue when supporting a large number of end devices that access the shared channels randomly. The scalability of LoRa networks greatly depends on the spreading factor (SF) allocation schemes. In this article, we propose an exponential windowing scheme (EWS) for LoRa networks to improve the scalability of LoRa networks. EWS is a distance-based SF allocation scheme. It assigns a distance parameter to each SF to maximize the success probability of the overall LoRa network. Using stochastic geometry, expressions for success probability are derived under co-SF interference. The impact of exponential windowing and packet size is analyzed on packet success probability. In addition, the proposed scheme is compared with the existing distance-based SF allocation schemes: equal-interval-based and equal-area-based schemes, and it is shown that the proposed scheme performs better than the other two schemes.**

Index Terms—**Long range (LoRa) network, LoRaWAN, scalability, spreading factor (SF) assignment, stochastic geometry.**

I. INTRODUCTION

LOW-POWER wide-area network (LPWAN) technologies have gained significant attention in the Internet-of-Things (IoT) community because of their capability to provide wide coverage to the low-power end devices (EDs) [1]–[3]. Some of the popular LPWAN technologies are SigFox and Long Range (LoRa) [4], [5]. Although, these technologies have their own benefits and limitations, LoRa is being considered as the most suitable among all the LPWAN technologies because of its open standard that enables us to set up an autonomous network [6], [7]. Moreover, LoRa is based on chirp spread spectrum (CSS) modulation, which makes the LoRa technology resistant to interference, since the chirp signal varies its frequency linearly with time [8]–[10]. CSS modulation uses different spreading factors (SFs) ranging from 7 to 12. Practically, SF defines the slope of chirp signals. Due to distinct slopes at different SF values, LoRa can support multiple simultaneous transmissions from different SF at the same frequency band.

Even though LoRa is being considered as the prime choice for IoT connectivity, it suffers from the problem of scalability when supporting large number of EDs simultaneously [11]. This is due to the fact that LoRa wide-area networks (LoRaWANs)[1] are based on an unslotted ALOHA protocol that accesses the shared channels randomly. Moreover, the transmission over the same SFs leads to interference known as co-SF interference [12], [13]. Hence, there is a high probability of packet collision over the same SFs. This results in a high packet loss rate and limits the LoRa scalability [8], [14]. In this article, our focus is on improving the scalability of the LoRa network. The scalability of LoRa network greatly depends on the SF allocation schemes [12]. We propose a novel distance-based SF allocation scheme, which improve the scalability of LoRa network with respect to the existing distance-based SF allocation schemes. A brief review of related existing works on scalability analysis of the LoRa network and how our proposed work differs from these existing works is introduced as follows.

II. RELATED WORKS AND CONTRIBUTIONS

The scalability of LoRa network based on different SF allocation schemes has been investigated in [12], [15]–[24]. In particular, the authors in [12] studied the scalability of LoRa network based on an equal-interval-based (EIB) scheme. Similarly, Georgiou and Raza in [15] studied the impact of LoRa scalability based on EIB and an equal-area-based (EAB) scheme. In both the EIB and EAB schemes, the total cell area is divided into K co-centered annulus, where the width of each annulus is determined by the allocation scheme, i.e., an equal width for EIB scheme and an equal area for EAB scheme. The SFs are assigned to EDs based on their distance from the gateway. The EDs lying in the annulus nearer to the gateway are assigned lowest SF, and the

[1]LoRaWAN is the standard medium access control (MAC) layer protocol for handling communication between LPWAN gateways and EDs.

SF is incremented by one for each subsequent annulus. Van den Abeele *et al.* [16] analyzed the scalability of the LoRa network using network simulator-3. Mahmood *et al.* [17] analyzed the scalability of the LoRa network based on EIB and EAB schemes under imperfect orthogonality among different SFs. Similarly, the scalability of LoRa networks based on EIB scheme under inter-SF interference has been studied in [18] and [19]. Recently, Hou *et al.* [20] proposed a MAC layer protocol for LoRaWAN and analyzed the performance of the LoRa network considering random, EIB and EAB SF allocation schemes. Likewise, Hoeller *et al.* [21] considered distance-based SF allocation, and derived an analytical expression for the outage probability. Beltramelli *et al.* [22] analyzed the scalability of the LoRa network for three different random access protocols, including unslotted ALOHA, pure ALOHA, and nonpersistent carrier-sense multiple access protocols. These schemes also consider the EIB and EAB SF allocation schemes. Tiurlikova *et al.* [23] attempt to find out the number of EDs assigned to each SF so as to maximize the packet delivery rate. However, this article is based on the assumption that all EDs are located at the fixed distance from the gateway. Furthermore, this work does not take into account the capture effect.[2]

Apart from these schemes, the work in [25] has analyzed the scalability of LoRa network based on receiver sensitivity. While Cuomo *et al.* [26] have proposed SF allocation schemes based on the received signal strength indicator (RSSI) and time-on-air (ToA) parameter. These schemes are specifically focused on the throughput of the LoRa network while they neglected the scalability of the LoRa network in terms of packet success probability. Similarly, Khalifeh *et al.* [27] proposed the throughput-centered SF allocation algorithm. While Farhad *et al.* [28] proposed an SF allocation scheme based on ToA parameter. Zhu *et al.* [29] proposed a tree-based SF allocation scheme for the multihop LoRa network. While Reynders *et al.* [30] proposed scheduling-based algorithm, where the gateway sends a beacon signal before the transmission of packets to avoid collision. This algorithm randomly allocates SF to each ED, hence limits the scalability of LoRa network. Similarly, in [31] and [32], the authors proposed the scheduling schemes to avoid the collision in LoRaWAN. However, these scheduling algorithms ([30]–[32]) cannot adapt to the requirements of LoRaWAN, as they may introduce excessive communication overhead, EDs cost, power consumption (because the beacon signal requires additional power to avoid collisions), and hardware complexity.

The work in [33] analyzed the performance of the LoRa network in terms of symbol error rate. However, the authors in this work does not take into account the impact of interference, whereas Fawaz *et al.* [34] proposed the SF allocation algorithms in a multioperator deployment scenario. In contrast, the SF allocation scheme based on machine learning techniques (support vector machine and decision tree classifier) is proposed in [35]. In [36] and [37], the authors proposed adaptive data rate (ADR) algorithms that consider the SF assignment based on the average

signal-to-noise-ratio value of the measurements performed over the last 20 packets received from the ED. However, these algorithms do not include the features to reduce collisions. Recently, Marini *et al.* [38] proposed a collision-aware SF allocation algorithm (not taking into account the capture effect) for LoRaWAN. The authors claim that their algorithm performs better than the ADR algorithms proposed in [36] and [37]. However, we claim that our algorithm also outperforms this benchmark ([38]), since our algorithm includes the feature to select the best combination of allocating SFs to EDs based on the maximum packet success probability, taking into account the capture effect, not considered in [38]. Moreover, the algorithm proposed in [38] is applicable only for fixed packet sizes (PSs) of EDs and single-channel scenarios, whereas our proposed algorithm is even applicable for different PSs of EDs and multichannel scenarios. Based on the literature survey, the novelty of our article is listed as follows.

1) It is evident from the literature (viz., [12], [15]–[23]) that the distance-based SF allocation schemes have significantly impacted the scalability of LoRa networks (especially, EIB and EAB schemes). These SF allocation schemes allocate SF based on a fixed strategy, that is, they allocate SF based on either the equal width or the equal area. Due to the lack of flexibility in allocating SF based on fixed strategy,[3] the scalability of these schemes is limited. However, the scalability can be improved by assigning a suitable distance parameter to each SF. In this article, we proposed a flexible and generalized distance-based SF allocation scheme [called exponential windowing scheme (EWS)] to improve the scalability of LoRa networks. EWS is based on a tunable parameter known as the exponential factor, which defines the area allocated to different SFs. The EIB scheme can be considered as the special case of the proposed scheme.

2) SF allocation schemes presented in the literature do not take into account the capture effect in SF allocation. Therefore, these schemes rarely select the best combination of allocating SF to ED, whereas our proposed SF allocation scheme always selects the best combination of allocating SFs to EDs based on the maximum packet success probability, taking into account the capture effect.

3) Moreover, the existing works on SF allocation analyzed the scalability of the LoRa network for fixed value of parameters (i.e., fixed value of PSs, cell-radius, and number of EDs). They do not provide information about the required change in SF allocation, as per the change in these parameters. However, we propose a scheme that provides information on the required changes in SF allocation according to the change in these parameters. In particular, our proposed scheme provides the best combination of allocating SFs to EDs for different parameters based on maximum packet success probability.

Contributions: The main contributions of this article can be summarized as follows.

---

[2]Capture effect: even in the presence of collisions, there is a possibility that the gateway is able to capture the frame if the signal-to-interference ratio (SIR) is above a given threshold (capture threshold) [17].

[3]The fixed distance-based strategy signifies that the distance parameters set for SF allocation are the same regardless of ED density and PS.

1) We propose a generalized SF allocation scheme for the LoRa network called EWS. In EWS, area allocated to one SF is a times the area allocated to previous SF, where a is an exponential scaling factor. Note that $a > 0$.

2) Using stochastic geometry, we derive the packet success probability expression for the proposed scheme under the co-SF interference scenario.[4]

3) We analyze the impact of exponential factor "a" on the average packet success probability. We have considered both low density and high density of EDs. For low-density scenario, it is shown that large number of EDs should be assigned a lower SF. For high-density scenario, it is shown that the value of exponential factor corresponding to the maximum packet success probability decreases with an increase in ED density. In other words, with increase in ED density, some EDs shift from lower SF to higher SF.

4) It is shown that EIB scheme is the special cases of the proposed EWS. Moreover, it is shown that the EWS outperforms both the EIB and EAB schemes in terms of packet success probability.

5) Moreover, we analyze the scalability of our proposed work under a multichannel scenario. We also discuss the practical aspects involved in the implementation of our proposed work.

The rest of this article is organized as follows. Section III presents our system model, where special emphasis is given on the packet collision model. Section IV elaborates the proposed scheme and derives the expression for success probability. Results with discussion (including the analysis for same and different LoRa PSs of EDs, single-channel and multichannel scenarios, etc.) are presented in Section V. Section VI presents the implementation steps of proposed work in real scenarios. Finally, Section VII concludes this article.

III. SYSTEM MODEL

We have considered an uplink model for a single-gateway LoRa network in the presence of co-SF interference. A description of the system model is given as follows.

1) A gateway is assumed to be located at the origin of the cell. The EDs are spatially distributed in two-dimensional space according to homogeneous Poisson point process (PPP) ϕ with density $\lambda = \frac{\hat{N}}{\pi R^2}$ [17], [22]. Here, $\hat{N}$ denotes the mean of Poisson random variable N, where N defines the number of EDs in the cell, and R denotes the cell radius.

2) We have considered a Rayleigh fading between gateway and EDs [15], [17], [22].

3) We have considered the saturation mode of ALOHA transmission, which signifies that there is always a packet

to transmit. However, the packet transmission occurs based on duty-cycle constraints. This mean that the transmission considered is strictly periodic in the case of one subband (single-channel scenario), whereas it is a combination of multiple periodic processes in the case of several subbands (multichannel scenario). For simplicity, an analytical framework is developed for single channel (i.e., it is assumed that all the EDs are transmitting on the same channel using one of the SFs.) However, we have presented the simulations for the multichannel scenarios.

4) We have considered the packet transmission in only up-link mode (i.e., simplex nature of LoRaWAN gateways). It means the packet transmissions in uplink mode do not interfere with the packet transmissions in downlink mode. This assumption is quite valid, since there are separate channels for uplink and downlink in LoRa network [40].

The values of the various LoRa parameters for different SFs (i.e., SF7 to SF12) are shown in Table I . Note that the values of the packet duration are shown for 10-B packet.

In the next section, we consider the collision overlap model for LoRa packet transmission.

A. Collision Overlap Time

LoRa transmission is based on unslotted ALOHA, and hence even for a small packet duration, there is always a finite probability of packet collision (overlap) [14]. In the following proposition, we obtained the probability density function (pdf) of collision overlap time under co-SF interference. We considered interference from such LoRa networks, which shared the same spectrum. Note that, for mathematical tractability, we assumed that all the EDs have same PS. However, we have presented the simulation results to discuss the case where different EDs have different PSs.

Proposition 1: The pdf of collision overlap time under co-SF interference is given by

$$f_{t_{o,\kappa}}(t) = \left(1 - \frac{t_{p,\kappa}(2T_c - t_{p,\kappa})}{T_c^2}\right)\delta(t) + \frac{2t}{T_c^2} + \frac{2}{T_c}\left(1 - \frac{t_{p,\kappa}}{T_c}\right) \tag{1}$$

where $\delta(.)$ is the Dirac delta function, $t_{p,\kappa}$ denotes the packet duration corresponding to the κth annulus, $t_{o,\kappa}$ denotes the collision overlap time from the co-SF interferers, and T_c defines the contention time period.[5]

TABLE I
LoRa PARAMETERS WITH THEIR VALUE

SF s	Annuli (κ)	Data-rate (kbps)	Packet Duration $t_{p,\kappa}$ (sec)	Receiver Sensitivity σ_s (dBm)	Range (r_κ)
7	1	5.47	0.036	-123	$[r_0, r_1]$
8	2	3.13	0.062	-126	$[r_1, r_2]$
9	3	1.76	0.124	-129	$[r_2, r_3]$
10	4	0.98	0.248	-132	$[r_3, r_4]$
11	5	0.54	0.414	-134.5	$[r_4, r_5]$
12	6	0.29	0.827	-137	$[r_5, r_6]$

---

[4]The reason for considering the co-SF interference follows from the concept of LoRa orthogonality [39], which states that the signals that are transmitted with different chirp slopes are always orthogonal. Mathematically, the chirp slope (Δ_c) is defined as: $\Delta_c = \frac{B^2}{2^{SF}}$, where B defines the bandwidth, whereas SF defines the spreading factor. Note that the value of bandwidth is fixed for the region. For example, the bandwidth assigned to Europe region is 125 kHz. Hence, the notion of considering co-SF interference is quite valid.

[5]It is the time-duration over which the performance of LoRa network is analyzed based on packet transmissions and their associated collisions. Within T_c, EDs transmit their packets randomly using unslotted ALOHA protocol.
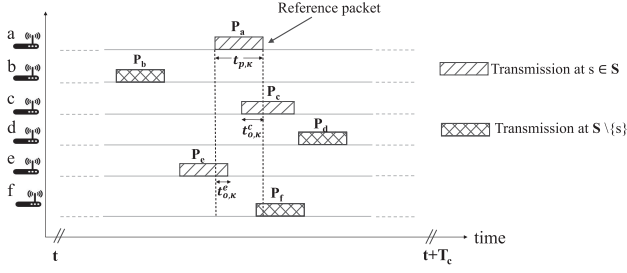
Fig. 1. Illustration of packet transmission in unslotted ALOHA and associated packet collision.

TABLE II
EU863-870 MHz BAND DUTY-CYCLE LIMITATIONS [41]

Sub Band	Frequency Band (MHz)	Duty-cycle (per sub-band)	Number of Available Channels	Channel Number	Duty-cycle (per channel)
h1.4	EU 868-868.6	1 %	3	#1	0.333 %
				#2	0.333 %
				#3	0.333 %
h1.5	EU 868.70-869.20	0.1 %	2	#4	0.05 %
				#5	0.05 %
h1.6	EU 869.40-869.65	10 %	1	#6	10 %
h1.7	EU 869.70-870	1 %	1	#7	1 %

Proof: See Appendix A for the proof. ∎

Note that the first term on the right-hand side of (1) defines the case when there is no collision of packets. While the second and third terms define the packet collisions case. This proposition is used in a later study for the analysis of packet success probability to obtain the average results with respect to collision overlap duration. Now, we define the SIR of an ED at the gateway for an uplink scenario.

The SIR η_κ experienced by typical ED, from the κth annulus, at the gateway under co-SF interference is given by

$$\eta_\kappa = \frac{A_0 \, g d^{-\alpha}}{I_\kappa}, \qquad I_\kappa = \sum_{j \in \phi_\kappa / S_0} A_0 g_j d_j^{-\alpha} \frac{t_{o,\kappa}}{t_{p,\kappa}} \qquad (2)$$

where $A_0 = (\frac{c}{4\pi f_c})^2$, which comes from Friis transmission equation with carrier frequency f_c, and velocity of light c. Here, g and g_j denote fading channel gain from gateway to the typical ED and jth interfering ED, respectively. The distances from the gateway to typical ED and interfering ED are denoted by d and d_j, respectively. Note that ϕ_κ / S_0 denotes the set of all active EDs except the typical ED (S_0) corresponding to the κth annulus. The factor $\frac{t_{o,\kappa}}{t_{p,\kappa}}$ is used to normalize the interference power [15]. This is because the packet collision depends on the overlapped duration of κth interfering packet ($t_{o,\kappa}$) and packet duration ($t_{p,\kappa}$), where $t_{o,\kappa}$ is most likely lesser than $t_{p,\kappa}$. Hence, we need to normalize interfering power value by the factor $\frac{t_{o,\kappa}}{t_{p,\kappa}}$.

A visual picture of packet transmission in unslotted ALOHA and associated packet collision is shown in Fig. 1. It considers six LoRa EDs (i.e., $a, b, \ldots, f$). Each transmits their packets randomly within the contention time period of T_c using unslotted ALOHA protocol. In the figure, the packet of ED a (denoted by P_a) with SF s is considered as reference packet. For the given example, packet of ED c (denoted by P_c) and packet of ED e (denoted by P_e) overlap with the P_a since they are transmitting at the same SF s. Hence, the interference I_a for a reference packet P_a under co-SF interference can be modeled as $I_a = \frac{t_{o,\kappa}}{t_{p,\kappa}} A_0 g_c d_c^{-\alpha} + \frac{t_{o,\kappa}}{t_{p,\kappa}} A_0 g_e d_e^{-\alpha}$.

B. Duty-Cycle Constraints

Duty-cycle constraints set a lower bound on waiting time between two successive packet transmissions of the same ED [17]. The waiting time between two successive packet transmissions

of the same ED is calculated based on the parameters, including duty-cycle constraint and packet duration. For example, duty-cycle constraint of 1% means that after its initial packet transmission within T_c, EDs must wait for the 99% of the packet duration for the next packet transmission. Since, the packet duration varies with SFs and PSs, then for a fixed duty-cycle constraint, the EDs waiting time between two successive packet transmissions of the same ED also varies with SFs and PSs. For a duty-cycle constraint of 1%, the waiting time between two successive packet transmission of the same ED for different SFs and PSs is defined by elements of matrix τ_w, given in (3). Where each element of the matrix specifies the wait time between two successive packet transmissions of same ED corresponding to a certain combination of PS and SF

$\tau_w(\text{sec})$

$$= \begin{pmatrix} & SF_7 & SF_8 & SF_9 & SF_{10} & SF_{11} & SF_{12} \\ PS_{10} & 3.564 & 6.138 & 12.276 & 24.552 & 40.986 & 81.873 \\ PS_{20} & 4.554 & 9.207 & 16.335 & 32.571 & 57.222 & 114.35 \\ PS_{25} & 5.643 & 10.197 & 18.315 & 36.729 & 65.241 & 130.58 \\ PS_{30} & 6.138 & 11.187 & 20.394 & 40.788 & 73.359 & 146.72 \\ PS_{40} & 7.623 & 14.157 & 26.433 & 48.906 & 89.595 & 163.05 \\ PS_{50} & 9.108 & 16.236 & 30.492 & 56.925 & 105.83 & 195.43 \end{pmatrix}$$

$$(3)$$

$\hat{\tau}_w(\text{sec})$

$$= \begin{pmatrix} & SF_7 & SF_8 & SF_9 & SF_{10} & SF_{11} & SF_{12} \\ h1.4 & 3.564 & 6.138 & 12.276 & 24.552 & 40.986 & 81.873 \\ h1.5 & 3.596 & 6.194 & 12.388 & 24.78 & 41.36 & 82.62 \\ h1.6 & 3.240 & 5.580 & 11.160 & 22.320 & 37.260 & 74.43 \\ h1.7 & 3.564 & 6.138 & 12.276 & 24.552 & 40.986 & 81.873 \end{pmatrix}.$$

$$(4)$$

Duty-cycle constraints under multichannel scenario: the duty-cycle constraints of available subbands at EU863-870 MHz band are different [17], [41]. These duty-cycle constraints in the four subbands are shown in Table II. The maximum values of duty-cycle allowed for EU863-870 MHz band are 0.1%, 1%, and 10% depending on the subbands (see Table II). To present the results for multichannel scenarios, these duty-cycle constraints (i.e., waiting time between two successive packet transmissions of same ED) of different subbands must be taken into account. For different SFs and subbands at EU863-870 MHz ISM band, the waiting time between two successive packet transmissions of the same ED is defined by elements of matrix $\hat{\tau}_w$ [given in (4)]. Where each entry of matrix specifies the wait time between two
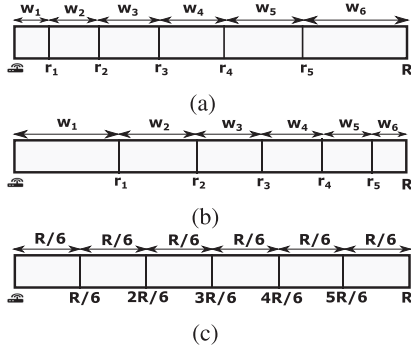
Fig. 2. Illustration depicting the variation of the parameters r_κ and w_κ for three different ranges of a. (a) $a < 1$. (b) $a > 1$. (c) $a = 1$

Fig. 4. Packet success probability variation with respect to a for different number of EDs. Here, PS $= 10$ B and $R = 15$ km. (a) Low-density scenario. (b) High-density scenario.
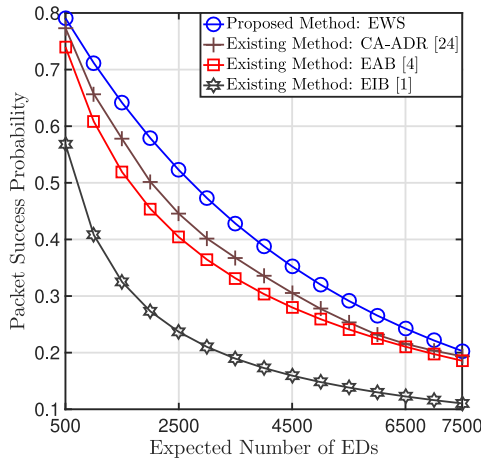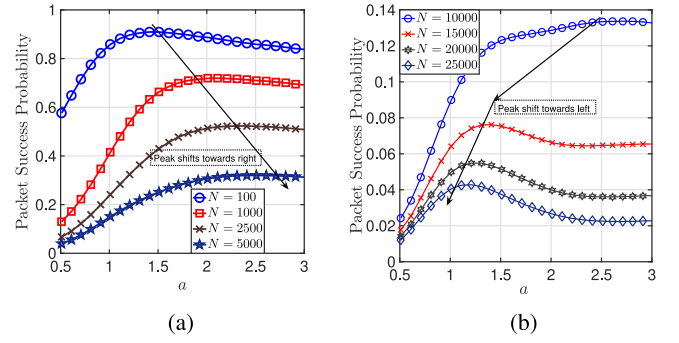

Fig. 3. Packet success probability versus N for EIB, EAB, and proposed schemes. Here, PS $= 10$ B and $R = 15$ km.

successive packet transmissions of same ED corresponding to a certain combination of subband and SF. Note that the entries of matrix are defined for a PS of 10 B.

IV. PROPOSED SCHEME

In this section, we present the proposed SF allocation scheme, i.e., EWS, and derive the expression of packet success probability under co-SF interference.

A. Exponential Windowing Scheme

EWS involves three phases: Windowing, SF assignment, and selecting the distance parameter.

1) Windowing: Initially, this scheme divides the cell radius (R) into K parts, where K denotes the total number of annuli (windows). The width of each window depends upon the value of exponential scaling factor, "a." Based on value of a, there can be three possible cases of dividing R: Case 1: $a < 1$ [see Fig. 2(a)], Case 2: $a > 1$ [see Fig. 2(b)], and Case 3: $a = 1$ [see Fig. 2(c)]. Note that a is nonnegative variable. Mathematically, the width of each annulus κ varies as given by the following

relation:

$$w_\kappa = a^{6-\kappa}W, \qquad \kappa = 1, 2, \ldots, K \qquad (5)$$

where

$$W = \begin{cases} \frac{R(1-a)}{1-a^6}; & a < 1 \\ \frac{R(a-1)}{a^6-1}; & a > 1 \\ \frac{R}{6}; & a = 1 \end{cases} \qquad (6)$$

The expression of width in (5) is derived as follows. The width of each window w_κ (where $\kappa = \{1, 2, \ldots, K\}$) depends on the tunable parameter known as the exponential scaling factor a. Note that the parameter K defines the cardinality of the set of SF, i.e., $K = |\kappa| = 6$ for SF ranging from 7 to 12. The width of rightmost window is considered to be W, i.e., $w_6 = W$ (see Fig. 2). Then, according to our proposed EWS, the width of subsequent windows is scaled by factor of a, i.e., $w_5 = aW$, $w_4 = a^2 W$, $w_3 = a^3 W$, $w_2 = a^4 W$, and $w_1 = a^5 W$. Hence, in generalized form, the width of each window can be defined as given by (5),[6] where the expression of W can be obtained as follows. The sum of width of these windows is equal to the cell radius (R), that is

$$R = w_1 + w_2 + w_3 + w_4 + w_5 + w_6$$
$$= (a^5 + a^4 + a^3 + a^2 + a + 1)W. \qquad (7)$$

Note that the width of windows forms a geometric progression (GP) series. Hence, following the formula for the sum of terms in a GP, one can obtain the expression of W, as given by (6).

A visual picture of windowing for all three cases of a is shown in Fig. 2, where the parameter r_κ (where $\kappa = \{1, 2, \ldots, K\}$) defines the distance from gateway to the outer boundary of κth annulus. Fig. 2(a) depicts the variation of parameter w_κ for $a < 1$. Note that, for such a case, the window nearest to gateway has the smallest width (denoted by w_1) among all other windows. The width of subsequent windows increases by a factor of a. In contrast, for $a > 1$ [see Fig. 2(b)], the window nearest to gateway has the largest width (denoted by w_1) among all other windows. The width of the subsequent windows decreases by the factor a.

---

[6]Note that the number 6 in the power of a is due to the fact that the total number of considered SFs are 6.

Fig. 2(c) is equivalent to the EIB scheme. It divides R into equal widths irrespective of the distance from the gateway.

2) SF Assignment: The next step is to assign SF to each ED based on windowing. First, assign the lowest SF (SF7) to the window which is nearest to the gateway. All the EDs lie under this window are assigned SF7. Then, assign the next higher SF (SF8) to the next window (i.e., the window which is next to the nearest window), and so on. The width shared by each SF is related to the range of a. The value $a < 1$ signifies that the larger portion of the entire width is shared by higher SFs [see Fig. 2(a)]. In other words, larger number of EDs are assigned a higher SFs. The value $a > 1$ signifies that the larger portion of the entire width is shared by lower SFs [see in Fig. 2(b)]. In other words, the higher number of EDs will be assigned a lower SFs. The value $a = 1$ [see Fig. 2(c)] signifies that the entire width is equally shared by each SF, which corresponds to the EIB SF allocation scheme. Hence, EIB SF allocation scheme can be considered as the special case of proposed SF allocation scheme.

3) Selecting the Distance Parameter: The next step is to find the r_κ parameter[7] for which the success probability of the LoRa system is maximum. This scheme considers the variation of r_κ parameter and seeks the value of r_κ for which maximum success probability is achieved.

B. Packet Success Probability

Packet success probability of LoRa network defines the number of EDs that can be successfully decoded at the gateway. The packet with SF s (or annulus κ, where $\kappa \in \{1, 2, \ldots, K\}$) will be successfully decoded at the gateway, if it satisfies the following two conditions: (I) the received power at gateway must be greater than the receiver sensitivity (σ_s): $PA_o g d^{-\alpha} > \sigma_s$ where P denotes the transmit power of each ED, and (II) the SIR (η_κ) experienced by packets of annulus κ must be greater than the target SIR (δ_κ) corresponding to κth annulus under co-SF interference: $\eta_\kappa > \delta_\kappa$.

The success probability of a packet for SF s (annulus κ) located at distance d from the gateway is given as

$$PSP(d, \delta_\kappa) = \mathbb{P}\{[\eta_\kappa > \delta_\kappa] \cap [PA_0 \, g d^{-\alpha} > \sigma_s]\}$$
$$\overset{(a)}{\geq} \mathbb{P}[\eta_\kappa > \delta_\kappa] \cap \mathbb{P}[PA_0 \, g d^{-\alpha} > \sigma_s]. \quad (8)$$

The inequality in (a) holds because the conditional probability is greater than the unconditional probability. Note that the inequality is tight[8] for interference-limited scenario [42]. The first

---

[7]This parameter defines the distance from gateway to outer boundary of κth annulus, i.e., $r_\kappa = \sum_{i=1}^{\kappa} w_i$.
[8]An inequality is said to be tight if for some conditions the inequality converges to equality.

term in (8), $\mathbb{P}[\eta_\kappa > \delta_\kappa]$ can be derived as follows:

$$\mathbb{P}[\eta_\kappa > \delta_\kappa] = \mathbb{E}_{I_\kappa}\left[\mathbb{P}\left[\frac{A_0 \, g d^{-\alpha}}{I_\kappa} > \delta_\kappa\right]\right]$$
$$\overset{(b)}{=} \mathbb{E}_{I_\kappa}\left[\exp\left(\frac{-\delta_\kappa I_\kappa d^\alpha}{A_0}\right)\right] \quad (9)$$
$$\overset{(c)}{=} \mathcal{L}_{I_\kappa}\left(\frac{\delta_\kappa I_\kappa d^\alpha}{A_0}\right).$$

Here, (b) in (9) follows from the assumption that $g \sim \exp(1)$, whereas (c) follows from the definition of Laplace transform, where $\mathcal{L}_{I_\kappa}(.)$ denotes the Laplace transform of I_κ. Using Laplace transform definition, $\mathcal{L}_{I_\kappa}(s)$ can be given as

$$\mathcal{L}_{I_\kappa}(s) = \mathbb{E}[\exp(-sI_\kappa)]$$
$$= \mathbb{E}_{\phi_\kappa/S_0, g_j, t_{o,\kappa}}\left[\exp\left(-s \sum_{j \in \phi_\kappa/S_0} A_0 g_j d_j^{-\alpha} \frac{t_{o,\kappa}}{t_{p,\kappa}}\right)\right]$$
$$= \mathbb{E}_{\phi_\kappa/S_0, g_j, t_{o,\kappa}}\left[\prod_{j \in \phi_\kappa/S_0} \exp(-s g_j d_j^{-\alpha})\right] \quad (10)$$

where $s = \frac{\delta_\kappa d^\alpha}{A_0}$. Using moment generation function of exponential random variable with $g_j \sim \exp(1)$

$$\mathcal{L}_{I_\kappa}(s) = \mathbb{E}_{\phi_\kappa/S_0, t_{o,\kappa}}\left[\prod_{j \in \phi_\kappa/S_0} \frac{1}{1 + s A_0 d_j^{-\alpha} \frac{t_{o,\kappa}}{t_{p,\kappa}}}\right]$$
$$= \mathbb{E}_{\phi_\kappa/S_0}\left[\prod_{j \in \phi_\kappa/S_0} \mathbb{E}_{t_{o,\kappa}}\left[\frac{1}{1 + s A_0 d_j^{-\alpha} \frac{t_{o,\kappa}}{t_{p,\kappa}}}\right]\right]. \quad (11)$$

Using probability generating functional of homogeneous PPP [43], [44], we have

$$\mathcal{L}_{I_\kappa}(s) = \exp\left(-\beta\lambda \int_{\mathbb{R}^2}\left(1 - \mathbb{E}_{t_{o,\kappa}}\left[\frac{1}{1 + s A_0 x^{-\alpha} \frac{t_{o,\kappa}}{t_{p,\kappa}}}\right]\right) dx\right) \quad (12)$$

where β is the duty-cycle constraint parameter. The intensity of transmitting EDs at a given time is determined by the parameter β. The transformation of Cartesian to polar coordinates gives

$$\mathcal{L}_{I_\kappa}(s)$$
$$= \exp\left(-2\pi\beta\lambda \int_{r_\kappa}^{r_{\kappa+1}}\left(1 - \mathbb{E}_{t_{o,\kappa}}\left[\frac{1}{1 + s A_0 x^{-\alpha} \frac{t_{o,\kappa}}{t_{p,\kappa}}}\right]\right) x dx\right) \quad (13)$$

where r_κ defines the distance from gateway to outer boundary of κth annulus, and is given by $r_\kappa = \sum_{i=1}^{\kappa} w_i$

$$\mathbb{E}_{t_{o,\kappa}}\left[\frac{1}{1 + s A_0 x^{-\alpha} \frac{t_{o,\kappa}}{t_{p,\kappa}}}\right]$$
$$= \int_{t_{o,\kappa} \in T_c}\left[\frac{1}{1 + s A_0 x^{-\alpha} \frac{t_{o,\kappa}}{t_{p,\kappa}}} f_{t_{o,\kappa}}(t) dt_{o,\kappa}\right]. \quad (14)$$

Substituting (1) in (14), and then solving the integration of resulting expression, we get

$$
\mathbb{E}_{t_{o,\kappa}} \left[\frac{1}{1 + sA_0 x^{-\alpha} \frac{t_{o,\kappa}}{t_{p,\kappa}}} \right] = \left(1 - \frac{t_{o,\kappa}}{T_c^2}(2T_c - t_{o,\kappa}) \right) \delta(t)
$$
$$
+ \frac{2t_{o,\kappa} x^{\alpha}}{s^2 A_0^2 T_c^2} \left[\{A_0 T_c s - t_{o,\kappa}(x^{\alpha} + A_0 \, s)\} \log(1 + sA_0 x^{-\alpha}) \right].
$$
(15)

Now, replacing s with $\frac{\delta_\kappa d^\alpha}{A_0}$ in (15) and after some algebraic manipulations, we get

$$
\mathbb{E}_{t_{o,\kappa}} \left[\frac{1}{1 + \delta_\kappa \left(\frac{d}{x}\right)^\alpha \frac{t_{o,\kappa}}{t_{p,\kappa}}} \right] = \left(1 - \frac{t_{o,\kappa}}{T_c^2}(2T_c - t_{o,\kappa}) \right) \delta(t)
$$
$$
+ \frac{2t_{o,\kappa} x^\alpha}{\delta_\kappa^2 \, d^{2\alpha} T_c^2} \left[\{T_c \delta_\kappa d^\alpha - t_{o,\kappa}(x^\alpha + \delta_\kappa d^\alpha)\} \log(1 + \delta_\kappa \left(\frac{d}{x}\right)^\alpha) \right].
$$
(16)

Substituting (16) into (13), and then into (9), we obtain $\mathbb{P}[\eta_\kappa > \delta_\kappa]$. The second term of (8) is given by

$$
\mathbb{P}[PA_0 \, gd^{-\alpha} > \sigma_s] = \exp\left(-\frac{\sigma_s d^\alpha}{P} \right). \tag{17}
$$

The pdf of the distance of uniformly distributed random EDs in the area πR^2 is given by [15]

$$
f_D(d) = \frac{2\,d}{R^2}, \qquad d \le R. \tag{18}
$$

The packet success probability averaged over distance distribution of d ($f_D(d)$) is given by

$$
\text{PSP}_{\text{av}} = \sum_{\kappa \in K} \int_{r_\kappa}^{r_{\kappa+1}} \text{PSP}(d, \delta_\kappa) f_D(d) \mathrm{d}d. \tag{19}
$$

Substituting the resulting expression of (8) and (18) in (19), the average packet success probability can be obtained.

C. Optimization Problem Formulation and Solution

In this section, we formulate the packet success probability maximization problem as an optimization problem. Also, we proposed the heuristic solution to determine distance parameters (i.e., r_κ) corresponding to maximum packet success probability. The optimization problem is formulated as

$$
\underset{r_1, r_2, \dots, r_K}{\text{maximize}} \quad \text{PSP}_{\text{av}}
$$
$$
\text{subject to} \quad r_i \le r_{i+1} \quad \forall i \in \kappa \tag{20}
$$

where PSP_{av} is obtained in (17). However, using the following two assumptions viz., $\exp(-x) \approx 1 - x$ for small x, and considering the collision overlap case of $t_{o,\kappa} = 0$,[9] the formulated

---

[9]As this case covers the largest portion of the collision overlap process.

TABLE III
SIMULATION PARAMETERS

Parameters	Value
Transmit power of each ED (P)	14 dBm
Bandwidth (B)	125 KHz
Path-loss exponent (α)	3
Contention time period (T_c)	60 sec [15]
Target SIR (δ_κ)	1 dB [17]
Fading type	Rayleigh
Duty-cycle constraint (β)	1%

optimization problem can be approximated as follows:

$$
\underset{r_1, r_2, \dots, r_K}{\text{maximize}} \sum_{\kappa \in K} \left[\frac{r_{\kappa+1}^2 - r_\kappa^2}{R^2} - \frac{2\sigma_\kappa(r_{\kappa+1}^{\alpha+2} - r_\kappa^{\alpha+2})}{(\alpha+2)PA_oR^2} \right]
$$
$$
\times \left[1 - \pi\beta\lambda(r_{\kappa+1}^2 - r_\kappa^2) \frac{t_{o,\kappa}}{T_c^2}(2T_c - t_{o,\kappa}) \right]
$$
$$
\text{subject to} \quad r_i \le r_{i+1} \quad \forall i \in \kappa.
$$
(21)

For the noninteger value of α, (21) becomes a nonlinear programming problem. Our solution to the formulated problem considers the variation of exponential windowing factor and finds the value of the exponential windowing factor for which the maximum packet success probability is achieved. Then, based on the obtained value of the exponential factor (i.e., the value corresponding to maximum packet success probability), the distance parameter for each SF is calculated using (3) and (4), where these calculated distance parameters give the final solution for the formulated problem. However, one can also try this problem with a global optimization, viz., multilevel coordinate search. This can be a very good future work.

V. RESULTS AND DISCUSSION

In this section, we present the numerical results to analyze the scalability of the LoRa network for the proposed EWS. We performed the Monte Carlo simulations in MATLAB to obtain the results, where each simulation point is the averaged result of 10^5 iterations. We have considered the parameter values listed in Table III unless specified separately. Note that we have considered Rayleigh fading in simulation, therefore, corresponding power is given to be exponentially distributed with unit mean. For the simulations, we consider the LoRa gateway to be located at the center of a circle of radius R, whereas EDs are distributed in a circle according to PPP of intensity $\lambda = \frac{\hat{N}}{\pi R^2}$, where $\hat{N}$ denotes the average number of EDs. First, we divide the cell radius into K windows based on exponential scaling factor a [given by (3) and (4)], where K defines the cardinality of the set of SF. Here, we consider the set of SF ranging from 7 to 12, hence $K = 6$. Next, we assign SF to each ED based on windowing. We assign the SF7 to the window which is nearest to gateway and the SF8 to the next window, that is, the window which is next to the nearest window, and so on. Then, we obtain the SIR of the received packet at the gateway. The packet success probability is evaluated based on two conditions: first, the packet received power of desired signal is greater than the SF-dependent receiver

sensitivity, and second, the SIR of desired signal is greater than the predefined target SIR under co-SF interference scenario.

Fig. 3 compares the packet success probability of the proposed EWS with EIB scheme, EAB scheme, and collision-aware ADR (CA-ADR) algorithms, where the plotted results for the EIB and EAB schemes have been obtained using the notion of paper Georgiou and Raza [12] and Mahmood *et al.* [17], respectively. While the plotted results for CA-ADR algorithm have been obtained using the notion of paper Marini *et al.* [38]. The EIB and EAB schemes are introduced as follows.

1) EIB scheme [12]: The circular disc is divided into S concentric circles such that the width of each annulus is same, where the parameter K defines the cardinality of the set of SFs (κ), i.e., $K = |\kappa|$. The EIB scheme determines the width of annulus (w_κ), according to the relation $w_\kappa = \frac{R}{K}$.

2) EAB scheme [17]: The circular disc area is divided into K areas such that each annulus gets an equal area. The EAB scheme determines the width of annulus, according to $w_\kappa = R\sqrt{\frac{\kappa}{K}}$.

3) CA-ADR algorithm [38]: According to this algorithm, packet success probability calculation is based on [38, eq. 11] (i.e., $\mathbb{P}(s) = (1 - \frac{t_{p,s}}{T_c})^{2(N(s)-1)}$, where $t_{p,s}$ denotes the packet duration corresponding to SF s, $n(s)$ denotes the number of EDs using SF s, and T_c denotes the contention time period).

In these results, $R = 15$ km and PS of 10 B are taken to compute the packet success probability. It can be seen that the proposed scheme performs better than the other state-of-the-art schemes (EIB, EAB, and CA-ADR). In particular, for $N = 2500$, our analysis shows that EWS achieves a 55.25%, 23.5%, and 18.2% higher packet success probability than the EIB scheme, EAB scheme, and CA-ADR algorithm, respectively. The reason for the better performance of EWS than the EIB and EAB schemes is that EWS includes the feature to select the best combination of allocating SFs to EDs based on the maximum packet success probability, not considered in [12] and [17]. While the reason for the improved performance of EWS compared to the CA-ADR algorithm is that EWS takes into account the capture effect in SF allocation, which is not considered in [38].

Fig. 4 shows the variation of packet success probability with respect to "a" for different number of EDs. Fig. 4(a) considers the low-density scenario, whereas Fig. 4(b) considers the high-density scenario. Note that we define the low-density and high-density scenario based on the number of EDs distributed in a circle of fixed radius. According to Fig. 4(a), the scenario for which the number of EDs distributed in a circle of 15-km radius are less than 5000 is defined as low-density scenario. In terms of ED density, the scenario for which the number of EDs distributed per km^2 in a circle are less than $\frac{5000}{\pi \times 15^2}$ is defined as low-density scenario. While the scenario for which the number of EDs distributed per km^2 in a circle are greater than $\frac{5000}{\pi \times 15^2}$ is defined as high-density scenario. The following observations can be made from these results.

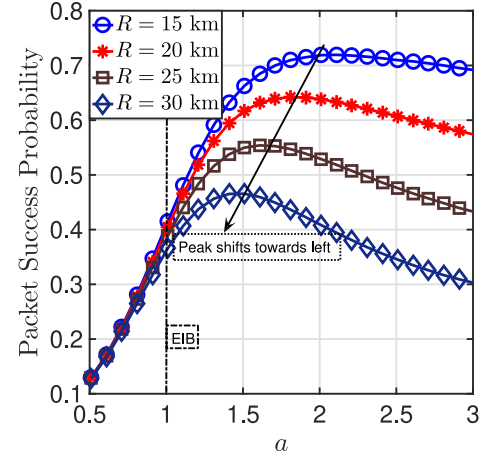1) The packet success probability first increases with the increase in the value of "a," maximum (peak) at a certain

Fig. 5. Packet success probability versus a for different values of cell radius (R). Here, PS = 10 bytes, $N = 1000$.

value of "*a*," and then decreases with a further increase in the value of "*a*." Note that the larger value of "*a*" signifies that larger area is assigned to lower SFs in comparison to higher SFs. Therefore, the observation can be interpreted in terms of area assigned to lower and higher SFs as follows: the packet success probability first increases with the increase in area assigned to lower SFs because the ToA for lower SF is small, and the collision probability is less. However, when large area is assigned to lower SF, co-SF interference dominates, which alleviates the gain provided by lower SF, hence the packet success probability decreases.

2) For low ED density scenario, it can be observed that the value of "*a*" corresponding to the maximum packet success probability increases with the increase in the number of EDs, that is, peak shifts toward right, as shown in Fig. 4(a). Hence, the obtained results signify that, in a low-density scenario, a large number of EDs can be assigned a lower SF. The reason is that the ToA for lower SF is small, and the collision probability is less for small ED density.

3) For high ED density scenario, it can be observed that the value of "*a*" corresponding to the maximum packet success probability decreases with the increase in N, that is, peak shifts toward left, as shown in Fig. 4(b). It signifies that with the increase in ED density, some EDs shift from lower SF to higher SF. The reason is that for large ED density, co-SF interference dominates, which alleviates the gain provided by lower SF.

From the aforementioned discussion, it can be concluded that in a low-density scenario, a large number of EDs can be assigned a lower SF to achieve the maximum packet success probability. While in a high-density scenario, a large number of EDs can be assigned a higher SF to achieve the maximum packet success probability.

Fig. 5 plots the packet success probability with respect to "*a*" for different values of R. It can be observed that the value of "*a*" corresponding to maximum packet success probability
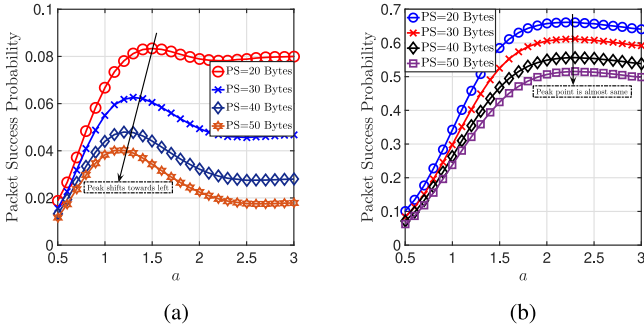
Fig. 6. Packet success probability variation with respect to a for different PSs. Here, $R = 15$ km. (a) $N = 10000$. (b) $N = 1000$.

Fig. 7. Packet success probability versus N for EIB, EAB, and EWS, when different users have different PSs. Here, PS $= 10$ B and $R = 15$ km.

decreases with increase in R. This happens because as R increases, it becomes difficult for lower SF EDs to satisfy condition (I) (the received power at gateway must be greater than the SF specific receiver sensitivity: $PA_o g d^{-\alpha} > \sigma_s$) for successful packet reception at the gateway. From the discussion, it can be concluded that the number of EDs assigned to higher SF increases with the increase in R.

A. Impact of LoRa PS on Success Probability and Exponential Factor

The ToA corresponding to each SF s can be calculated as follows:

$$\text{ToA}_s = t_{p,\kappa} = T_{\text{Preamble},s} + T_{\text{Payload},s} \tag{22}$$

where $T_{\text{Preamble},s}$ and $T_{\text{Payload},s}$ denote the preamble duration and payload duration, respectively. The preamble duration depends on symbol period (T_s) and number of preamble symbols (N_{Preamble}), and can be calculated as follows:

$$T_{\text{Preamble},s} = (N_{\text{Preamble}} + 4.25)T_s \tag{23}$$

where $T_s = \frac{2^s}{B}$. The payload duration corresponding to SF s can be calculated as [45]

$$T_{\text{Payload},s} = \left(8 + \max\left[\left\lceil \frac{8\text{PL} - 4s + 28 + 16\text{CRC} - 20H}{4(s - 2DE)} \right\rceil \right.\right.$$
$$\left.\left. \times (\text{CR} + 4), 0\right]\right) T_s \tag{24}$$

where PL denotes the payload length (in bytes). Here, H and DE are two flag variables where, H signifies whether the header is disabled ($H = 1$) or enabled ($H = 0$), whereas DE signifies whether the low data rate optimization is disabled (DE $= 0$) or enabled (DE $= 1$). CR denotes the coding rate that ranges from 1 to 4. Note that cyclic redundancy check (CRC) is enabled for CRC $= 1$ and disabled for CRC $= 0$. The default setting for LoRaWAN is CRC $= 1$.

Fig. 6 shows the variation of packet success probability with respect to a for different PSs (PS). Fig. 6(a) considers $N = 10000$, whereas Fig. 6(b) considers $N = 1000$. First, it can be seen that packet success probability decreases with the increase in PS. This is because ToA increases with increase in payload size, which further increases the probability of packet collisions.
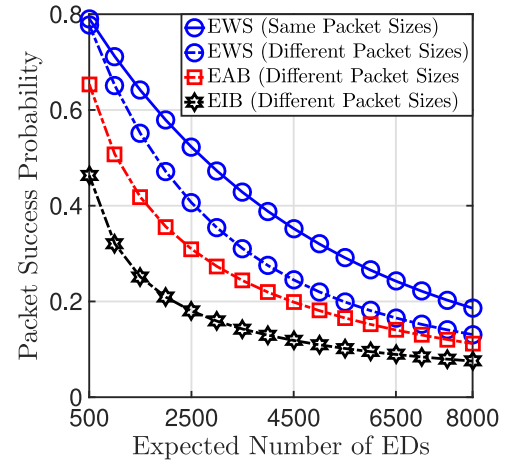
Also, it can be observed that as we increase the PS, the value of a corresponding to maximum success probability shifts toward left for $N = 10000$ [see Fig. 6(a)]. In other words, with an increase in PS, some of the EDs that were earlier served by lower SF shifted toward higher SF. This is due to the fact that as the size of packet increases, ToA (packet duration) also increases for the same SF, therefore some of the EDs shift from lower SFs to higher SFs. Note that, for $N = 1000$ [see Fig. 6(b)], the peak point is almost same for all PSs. This is because the collision probability is low for small ED density and ToA is small for low SF values.

B. Impact of Different PSs of EDs

To analyze the impact of different PSs of EDs on packet success probability, we perform the simulation considering LoRa packets of ten different PSs (ranging from 5 to 50 B). These PSs are defined by a set as: $S_p = \{5, 10, \ldots, 50\}$, where each element of the set defines the size of LoRa packet. We assume that EDs can select a LoRa packet of any size from the set S_p with equal probability.

Fig. 7 compare the packet success probability of the proposed EWS with EIB and EAB schemes for the case where different EDs have different PSs. It can be seen that, like the case of similar PSs of EDs, EWS performs better than both EIB and EAB schemes in the case of different PSs of EDs. In addition, Fig. 7 compare the packet success probability of EWS scheme under the same PSs and different PSs scenarios of EDs. It can be observed that under the same PSs scenario of EDs, EWS performs better than different PSs scenario of EDs.

C. Impact of Multichannels on Packet Success Probability

For the simulations under multichannel scenario, we consider the LoRa channel specifications of the Europe region in the EU863-870 MHz ISM band. The duty-cycle constraints of four
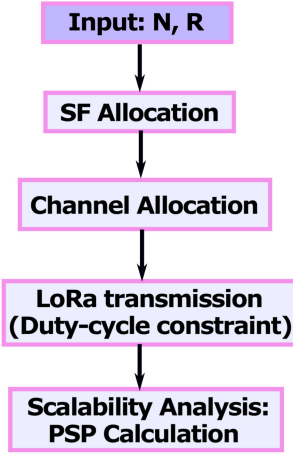
Fig. 8. Step-by-step process involved in the analysis for multichannel LoRa networks.
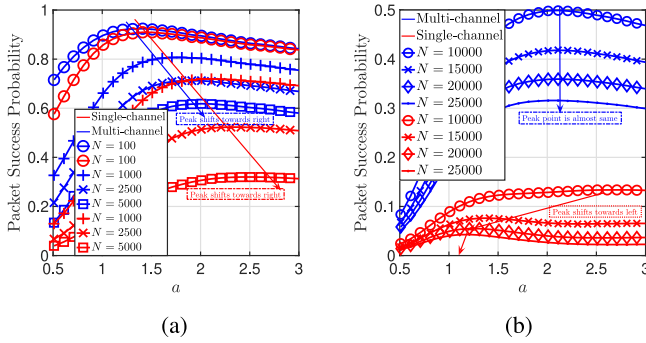

Fig. 10. Network throughput versus N for EIB, EAB, and EWS. Here, PS $= 10$ B and $R = 15$ km.

Fig. 9. Packet success probability variation with respect to a for multichannel scenario. Here, PS$= 10$ B and $R = 15$ km. (a) Low-density scenario. (b) High-density scenario.

subbands (or nonoverlapping seven uplink channels) available in the EU863-870 MHz ISM band are listed in Table II. A step-by-step process involved in our analysis for multichannel LoRa networks is provided in Fig. 8. First, each ED is allocated SF based on the EWS. Then, channel allocation is performed in a random fashion, i.e., the ED is equally likely to select one of the seven available channels. It is worth mentioning that the interference is significantly reduced compared to the single-channel scenario. The next step involves the transmission of packets based on duty-cycle limits defined in Table II. Finally, the scalability of LoRa network based on the considered SF allocation scheme is analyzed in terms of packet success probability. We analyze the scalability of multichannel scenario in terms of packet success probability and compare it with single-channel scenario. The variation in packet success probability with respect to a for low-density and high-density deployment of EDs is shown in Fig. 9(a) and (b), respectively. The following observations can be made from these results.

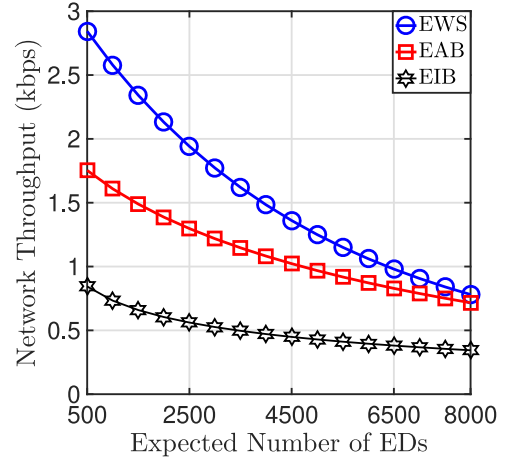1) The multichannel scenario has significantly high packet success probability than the single-channel scenario,

since the co-SF interference in multichannel scenario is significantly reduced.

2) For low-density deployment of EDs under multichannel scenario, the value of a corresponding to the maximum packet success probability increases with the increase in N. In other words, peak shifts toward right, as shown in Fig. 9(a).

3) For high-density deployment of EDs under multichannel scenario, the value of a corresponding to maximum packet success probability is almost same, as shown in Fig. 9(b), which signifies that same distance parameters are selected regardless of the value of N. The reason for this is that, in multichannel scenario, co-SF interference significantly reduces. Hence, high-density ED scenario behaves as low-density ED scenario of single-channel scenario [i.e., it behaves like Fig. 6(b)].

D. Network Throughput Analysis

The throughput ($\mathcal{T}$) of a LoRa networks depend on SF s, CR, and, bandwidth (B) of the communication channel [19], and it is expressed as

$$\mathcal{T} = s\frac{B}{2^s}CR. \tag{25}$$

The values of data rates for $B = 125$ kHz, $CR = \frac{4}{5}$, and different SFs (i.e., $s = \{7, 8, \ldots, 12\}$) are listed in Table I. These values of data rates are useful for calculating the throughput of LoRa networks under various SF allocation schemes. The network throughput for EWS, EIB, and EAB SF allocation schemes is calculated based on the following relation:

$$\mathcal{T} = \frac{1}{N} \sum_{s=\{7,8,\ldots,12\}} \hat{N}_s R_s \tag{26}$$

where N defines the total number of EDs in the cell, $\hat{N}_s$ defines the number of EDs assigned with SF s, and R_s defines the data rate corresponding to SF s. Fig. 10 compares the network

TABLE IV
SELECTION OF DISTANCE MEASUREMENT METHOD

Environment	LoS Scenario		NLoS Scenario	
Nature of Nodes	Static Nodes	Mobile Nodes	Static Nodes	Mobile Nodes
Applications	Assessment of potential tidal energy in sites at risk, monitoring activities in the marine environment, sea-to-ground communication	UAV tracking, ship tracking near sea	Smart metering, smart lighting, water quality monitoring	Items location tracking, animal tracking, vehicles tracking
Distance Measurement Methods	Using either of the given method	Using either (ii) or (iii) method	Using either (ii).(b) or (iii) method	Using (iii) method

throughput of the proposed EWS with EIB and EAB SF alloca-tion schemes. It can be seen that the proposed EWS has higher throughput than both EIB and EAB schemes. In particular, for $N = 2500$, our analysis shows that EWS achieves 245.8% higher throughput than the EAB scheme, whereas it achieves 49.55% higher throughput than the EAB scheme. The reason for the higher throughput of EWS is based on the fact that lower SFs has high data rate than the higher SFs. Also, in the same direction, EWS allocates relatively large number of EDs to lower SFs than in EIB and EAB schemes.

VI. PRACTICAL ASPECTS AND IMPLEMENTATION OF PROPOSED WORK

The proposed SF allocation scheme assign SFs based on the distance of EDs from the gateway. The key practical aspects involved in the implementation of our proposed scheme are discussed as follows.
1) Distance Measurement: The distance between EDs and gateway can be obtained using the following methods.
    i) Manually: Record the location of the gateway and ED at the time of their installation and calculate the distance accordingly.
    ii) Using RSSI values: We have discussed two methods for distance measurement based on RSSI values.
        a) RSSI-to-distance maps RSSI values [46]–[49].
        b) Averaging-based RSSI-to-distance mapping: this method follows the following steps.
            1) Measures the reading of RSSI at gateway from ED at different times.
            2) Perform the averaging operation on the readings measured in the previous step. Note that the number of readings must be such that averaging operation gives almost stabilized value of RSSI (i.e., variability is very less).
            3) Perform the RSSI-to-distance map-ping [46]–[49].
    (iii) Using global positioning system module on the devices.
    It is worth mentioning that all the aforementioned meth-ods are not applicable in all scenarios. However, the method(s) to be implemented based on the type of en-vironment (LoS or NLoS) and the nature of the nodes (stationary or moving) are given in Table IV. The appli-cations that come under stationary and moving node in LoS and NLoS scenarios are also listed in Table IV.

2) SF Allocation: The network server allocates SFs to EDs based on the proposed SF allocation scheme. Our SF allocation scheme checks both the necessary conditions for successful packet transmission, i.e., packet received power of desired signal is greater than the SF-dependent receiver sensitivity, and SIR of desired signal is greater than the predefined target SIR. Hence, it ensures that the best SF is assigned to each ED to reach its packet successfully at the gateway. However, packet transmis-sion becomes unsuccessful only when none of the avail-able SFs is capable of correctly reconstruct the receiver packet.
3) SF allocation updation mechanism: In the case of static LoRa nodes and fixed parameters setting (i.e., fixed num-ber of LoRa nodes, fixed cell-radius, and same PSs of EDs), the distance-parameters combination selected by EWS for allocating SFs remains the same. Therefore, in such a scenario, the network server needs to allocate SFs only once. However, in the case of static LoRa nodes with variable packets size transmissions, the distance-parameters combination selected by EWS for allocating SFs needs to be updated periodically. Essentially, SF allocation must be updated based on the packet dura-tion $t(\text{PS}_{\text{low}}, \text{SF}_{\text{low}})$ of lowest PS (PS_{low}) corresponding to lowest SF (SF_{low}) and its waiting time between two successive packet transmissions of the same ED ($\tau_{w,\text{low}}$). In particular, the network server will update the SF alloca-tion after every $T_{\text{upd}} = t(\text{PS}_{\text{low}}, \text{SF}_{\text{low}}) + \tau_{w,\text{low}}$ s. For in-stance, there are 1000 EDs (i.e., $N = 1000$) and each ED transmit a packet of any size from the PSs ranging from 10 to 50 B. So, $\text{PS}_{\text{low}} = 10$ B, $t(\text{PS}_{\text{low}}, \text{SF}_{\text{low}}) = 0.036$ s from Table I, and $\tau_{w,\text{low}} = 3.564$ for 1% duty-cycle [from matrix: (3)]. Then, the network server will update the SF allocation after every $T_{\text{upd}} = t(\text{PS}_{\text{low}}, \text{SF}_{\text{low}}) + \tau_{w,\text{low}}$ s. It is noteworthy that SF updation based on lower SF and lower PS also ensures the performance of higher SF along with the performance of lower SF. Following this way, the SF allocation updation mechanism ensures smooth updation taking into account all SFs and the PS of all EDs.
    Also, in the case of mobile LoRa nodes, network server follows the same updation mechanism as it follows in the case of static LoRa nodes with variable packets size transmissions.

A. Implementation of Proposed Work

The proposed work can be implemented in real scenarios as follows (key elements of LoRa networks are shown in Fig. 11). EDs send their packets to the gateway. LoRa gateway then for-ward uplink radio packets to LoRa network server. The gateway is connected to network server via Internet. The network server allocates the SFs to EDs based on the proposed SF allocation scheme as per the updation mechanism discussed earlier. The data are then sent via the Internet to the application server, which interprets and displays the received data.
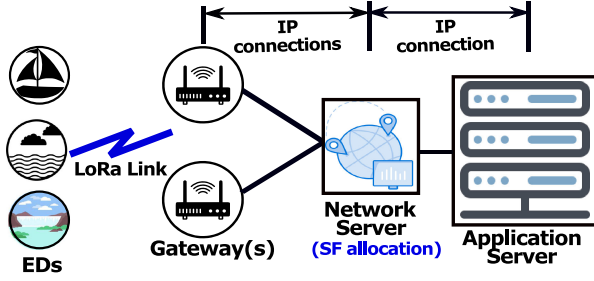
Fig. 11. Implementation of proposed work.

Fig. 12. Collision overlap cases. (a) No collision of packets. (b) Collision of packets.

VII. CONCLUSION

This article proposed a generalized SF allocation scheme to improve the scalability of LoRa networks. The proposed scheme provided information about when to switch from one SF to the next higher SF. Basically, it provided adaptability in selecting an appropriate SF based on ED density to maximize the packet success probability. Using stochastic geometry, the expression for the average success probability under the co-SF interference scenario was derived. In addition, we analyzed the impact of the exponential factor on the average packet success probability for different types of applications that consider sparse deployment (low-density) and dense deployment (high-density) of LoRa devices. Our analysis concluded that for low-density applications, including environment monitoring applications (such as forest monitoring, moisture measurement, and ground water quality monitoring), monitoring activities within the marine environment, etc., the devices should be served using lower SFs. While for high-density applications, including smart city applications (air-quality monitoring, waste management), smart agriculture applications, etc., the devices should be served using combinations of both lower and higher SFs. Also, we have compared the packet success probability for the proposed scheme with EIB and EAB SF allocation schemes, and it was shown that our proposed scheme performed better than the other two schemes. Moreover, we analyzed the impact of LoRa PS on success probability and the exponential factor. The analysis showed that for high-density applications, ToA increases with the increase in LoRa PS. Hence, the packet success probability decreases with the increase in LoRa PS. In this regard, our scheme also gave the information that the packet success probability was maximum when we assigned higher SFs to comparatively large number of EDs, than assigned in the case of smaller PS. The proposed work has numerous extensions, which are as follows.

1) Our model considered the single-gateway LoRa network. However, the model can be extended for multigateway LoRa network.
2) Our model considered the packet transmission in only uplink mode, however, it can be extended to take account the packet transmissions in both uplink and downlink modes.
3) Packet transmission in our model was based on the unslotted ALOHA protocol. However, our SF allocation schemes can also be extended to analyze the scalability for slotted ALOHA, and CSMA protocols.
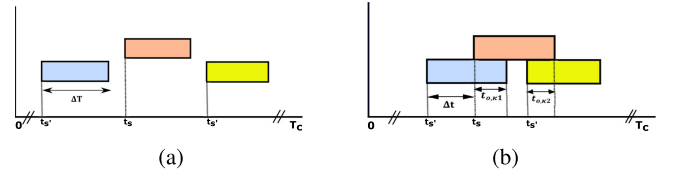
APPENDIX

A. Proof of Proposition 1

In unslotted ALOHA, each ED randomly transmits its packet within the contention time period (T_c). The transmission start time (denoted by t_s) of each ED can be modeled as a uniform distribution within T_c, i.e., $t_s \sim U(0, T_c - t_{p,\kappa})$. Since $T_c >> t_{p,\kappa}$, one can assume $t_s \sim U(0, T_c)$. In order to derive the pdf for collision overlap time, the following two cases have been considered (see Fig. 12): (a) when there is no collision of packets, and (b) when there is collision of packets (either complete overlapping or partial overlapping of packets). First, we obtain the pdf of difference of transmission start time of two colliding packets (t_s and $t_{s'}$), i.e., $\Delta T = t_s - t_{s'}$. Since the start times of both the colliding packets are uniformly distributed, the pdf of difference of two uniformly distributed random variables can be readily obtained by convolving the individual pdfs of both the packets. Therefore, the pdf of the difference of transmission start time of two colliding packets is given as

$$
f_{\Delta T}(t) = \begin{cases} \frac{1}{T_c}\left(1 + \frac{t}{T_c}\right); & -T_c < t < 0 \\ \frac{1}{T_c}\left(1 - \frac{t}{T_c}\right); & 0 < t < T_c \\ 0; & \text{otherwise} \end{cases} \quad . \quad (27)
$$

The cumulative distribution function (cdf) of $f_{\Delta T}(t)$ is given as

$$
F_{\Delta T}(t) = \begin{cases} \frac{1}{T_c}\left(t + \frac{t^2}{2T_c}\right); & -T_c < t < 0 \\ \frac{1}{T_c}\left(t - \frac{t^2}{2T_c}\right); & 0 < t < T_c \\ c; & \text{otherwise} \end{cases} \quad (28)
$$

where c is any constant. Now, we obtain the pdf for the case (a), i.e., when there is no collision of packets. For case (a), two conditions must be satisfied: $\Delta T > t_{p,\kappa}$ and $\Delta T < -t_{p,\kappa}$. The probability of $\Delta T > t_{p,\kappa}$ is given as

$$
\mathbb{P}(\Delta T > t_{p,\kappa}) = 1 - F_{\Delta T}(t_{p,\kappa}) = 1 - \frac{1}{T_c}\left[t_{p,\kappa} - \frac{t_{p,\kappa}^2}{2T_c}\right]. \quad (29)
$$

The probability of $\Delta T < -t_{p,\kappa}$ is given as

$$
\mathbb{P}(\Delta T < -t_{p,\kappa}) = F_{\Delta T}(-t_{p,\kappa}) = \frac{1}{T_c}\left[-t_{p,\kappa} + \frac{t_{p,\kappa}^2}{2T_c}\right]. \quad (30)
$$

Now, the probability that both the conditions are satisfied is given as

$$\mathbb{P}(\Delta T > t_{p,\kappa}) + \mathbb{P}(\Delta T < -t_{p,\kappa}) = \left(1 - \frac{t_{p,\kappa}}{T_c^2}(2T_c - t_{p,\kappa})\right). \tag{31}$$

Finally, the pdf for case (a) (let it be denoted by $f_{t'_{o,\kappa}}(t)$) can be given by

$$f_{t'_{o,\kappa}}(t) = \left(1 - \frac{t_{p,\kappa}}{T_c^2}(2T_c - t_{p,\kappa})\right)\delta(t). \tag{32}$$

Next, we obtain the pdf for case (b), i.e., when there is collision of packets (either complete overlapping or partial overlapping of packets). The cdf for the case (b) can be obtained using transformation of random variables ΔT and $t_{o,\kappa}$. For case (b), two conditions must be satisfied, i.e., $t_{o,\kappa 1} = t_{p,\kappa} - \Delta T$, and $t_{o,\kappa 2} = t_{p,\kappa} + \Delta T$, where $t_{o,\kappa 1}$ and $t_{o,\kappa 2}$ denote the collision overlapped time corresponding to two different conditions. The cdf for the condition $t_{o,\kappa 1} = t_{p,\kappa} - \Delta T$ can be derived as

$$\begin{aligned} F_{t_{o,\kappa 1}}(t) &= \mathbb{P}[t_{o,\kappa 1} \le t] = 1 - F_{\Delta T}(t_{p,\kappa} - t) \\ &= 1 - \frac{1}{T_c}\left[(t_{p,\kappa} - t) - \frac{(t_{p,\kappa} - t)^2}{2T_c}\right] \end{aligned} \tag{33}$$

and its pdf is given by

$$f_{t_{o,\kappa 1}}(t) = \frac{1}{T_c}\left[1 - \frac{t_{p,\kappa} - t}{T_c}\right]. \tag{34}$$

Similarly, the pdf for the condition $t_{o,\kappa 2} = t_{p,\kappa} + \Delta T$ can be calculated as

$$f_{t_{o,\kappa 2}}(t) = \frac{1}{T_c}\left[1 + \frac{t - t_{p,\kappa}}{T_c}\right]. \tag{35}$$

Adding (34) and (35), we obtain the pdf for case (b) (let it be denoted by $f_{t''_{o,\kappa}}(t)$), which is given by

$$f_{t''_{o,\kappa}}(t) = \frac{2t}{T_c^2} + \frac{2}{T_c}\left(1 - \frac{t_{p,\kappa}}{T_c}\right). \tag{36}$$

Finally, from (32) and (36), we obtain the overall pdf for the collision overlapped time as given in (1).

REFERENCES

[1] L. D. Xu, W. He, and S. Li, "Internet of Things in industries: A survey," *IEEE Trans. Ind. Informat.*, vol. 10, no. 4, pp. 2233–2243, Nov. 2014.

[2] M. Centenaro, L. Vangelista, A. Zanella, and M. Zorzi, "Long-range communications in unlicensed bands: The rising stars in the IoT and smart city scenarios," *IEEE Wireless Commun.*, vol. 23, no. 5, pp. 60–67, Oct. 2016.

[3] Z. Qin, F. Y. Li, G. Y. Li, J. A. McCann, and Q. Ni, "Low-power wide-area networks for sustainable IoT," *IEEE Wireless Commun.*, vol. 26, no. 3, pp. 140–145, Jun. 2019.

[4] Link Labs, "A comprehensive look at low power, wide area networks for Internet of Things engineers and decision makers," White Paper, 2016.

[5] A. Ikpehai *et al.*, "Low-power wide area network technologies for Internet-of-Things: A comparative review," *IEEE Internet Things J.*, vol. 6, no. 2, pp. 2225–2240, Apr. 2019.

[6] D. Magrin, M. Centenaro, and L. Vangelista, "Performance evaluation of LoRa networks in a smart city scenario," in *Proc. IEEE Int. Conf. Commun.*, 2017, pp. 1–7.

[7] J. P. S. Sundaram, W. Du, and Z. Zhao, "A survey on LoRa networking: Research problems, current solutions, and open issues," *IEEE Commun. Surv. Tut.*, vol. 22, no. 1, pp. 371–388, Jan.–Mar. 2020.

[8] F. Adelantado, X. Vilajosana, P. Tuset-Peiro, B. Martinez, J. Melia-Segui, and T. Watteyne, "Understanding the limits of LoRaWAN," *IEEE Commun. Mag.*, vol. 55, no. 9, pp. 34–40, Sep. 2017.

[9] M. Chiani and A. Elzanaty, "On the LoRa modulation for IoT: Waveform properties and spectral analysis," *IEEE Internet Things J.*, vol. 6, no. 5, pp. 8463–8470, Oct. 2019.

[10] N. Jovalekic, V. Drndarevic, I. Darby, M. Zennaro, E. Pietrosemoli, and F. Ricciato, "LoRa transceiver with improved characteristics," *IEEE Wireless Commun. Lett.*, vol. 7, no. 6, pp. 1058–1061, Dec. 2018.

[11] E. Sisinni *et al.*, "A LoRaWAN range extender for industrial IoT," *IEEE Trans. Ind. Informat.*, vol. 16, no. 8, pp. 5607–5616, Aug. 2020.

[12] O. Georgiou and U. Raza, "Low power wide area network analysis: Can LoRa scale?," *IEEE Wireless Commun. Lett.*, vol. 6, no. 2, pp. 162–165, Apr. 2017.

[13] Z. Qin, Y. Liu, G. Y. Li, and J. A. McCann, "Performance analysis of clustered LoRa networks," *IEEE Trans. Veh. Technol.*, vol. 68, no. 8, pp. 7616–7629, Aug. 2019.

[14] J. Markkula, K. Mikhaylov, and J. Haapola, "Simulating LoRaWAN: On importance of inter spreading factor interference and collision effect," in *Proc. IEEE Int. Conf. Commun.*, 2019, pp. 1–7.

[15] J. Lim and Y. Han, "Spreading factor allocation for massive connectivity in LoRa systems," *IEEE Commun. Lett.*, vol. 22, no. 4, pp. 800–803, Apr. 2018.

[16] F. Van den Abeele, J. Haxhibeqiri, I. Moerman, and J. Hoebeke, "Scalability analysis of large-scale LoRaWAN networks in NS-3," *IEEE Internet Things J.*, vol. 4, no. 6, pp. 2186–2198, Dec. 2017.

[17] A. Mahmood, E. Sisinni, L. Guntupalli, R. Rondón, S. A. Hassan, and M. Gidlund, "Scalability analysis of a LoRa network under imperfect orthogonality," *IEEE Trans. Ind. Informat.*, vol. 15, no. 3, pp. 1425–1436, Mar. 2019.

[18] D. Croce, M. Gucciardo, S. Mangione, G. Santaromita, and I. Tinnirello, "Impact of LoRa imperfect orthogonality: Analysis of link-level performance," *IEEE Commun. Lett.*, vol. 22, no. 4, pp. 796–799, Apr. 2018.

[19] A. Waret, M. Kaneko, A. Guitton, and N. El Rachkidy, "LoRa throughput analysis with imperfect spreading factor orthogonality," *IEEE Wireless Commun. Lett.*, vol. 8, no. 2, pp. 408–411, Apr. 2019.

[20] Y. Hou, Z. Liu, and D. Sun, "A novel MAC protocol exploiting concurrent transmissions for massive LoRa connectivity," *J. Commun. Netw.*, vol. 22, no. 2, pp. 108–117, 2020.

[21] A. Hoeller, R. D. Souza, S. Montejo-Sánchez, and H. Alves, "Performance analysis of single-cell adaptive data rate-enabled LoRaWAN," *IEEE Wireless Commun. Lett.*, vol. 9, no. 6, pp. 911–914, Jun. 2020.

[22] L. Beltramelli, A. Mahmood, P. Osterberg, and M. Gidlund, "LoRa beyond ALOHA: An investigation of alternative access protocols," *IEEE Trans. Ind. Informat.*, vol. 17, no. 5, pp. 3544–3554, May 2021.

[23] A. Tiurlikova, N. Stepanov, and K. Mikhaylov, "Method of assigning spreading factor to improve the scalability of the LoRaWan wide area network," in *Proc. 10th Int. Congr. Ultra Modern Telecommun. Control Syst. Workshops*, 2018, pp. 1–4.

[24] D. Saluja, R. Singh, L. K. Baghel, and S. Kumar, "Scalability analysis of LoRa network for SNR based SF allocation scheme," *IEEE Trans. Ind. Informat.*, to be published, doi: 10.1109/TII.2020.3042833.

[25] R. B. Sorensen, N. Razmi, J. J. Nielsen, and P. Popovski, "Analysis of LoRaWAN uplink with multiple demodulating paths and capture effect," in *Proc. IEEE Int. Conf. Commun.*, 2019, pp. 1–6.

[26] F. Cuomo *et al.*, "EXPLoRa: Extending the performance of LoRa by suitable spreading factor allocations," in *Proc. IEEE 13th Int. Conf. Wireless Mobile Comput., Netw. Commun.*, 2017, pp. 1–8.

[27] A. Khalifeh, S. Shraideh, and K. A. Darabkh, "Joint channel and spreading factor selection algorithm for LoRaWAN based networks," in *Proc. Int. Conf. U.K.-China Emerg. Technol.*, 2020, pp. 1–4.

[28] A. Farhad, D. Kim, P. Sthapit, and J. Pyun, "Interference-aware spreading factor assignment scheme for the massive LoRaWAN network," in *Proc. Int. Conf. Electron., Inf., Commun.*, 2019, pp. 1–2.

[29] G. Zhu, C. Liao, T. Sakdejayont, I. Lai, Y. Narusue, and H. Morikawa, "Improving the capacity of a mesh LoRa network by spreading-factor-based network clustering," *IEEE Access*, vol. 7, pp. 21584–21596, Feb. 2019.

[30] B. Reynders, Q. Wang, P. Tuset-Peiro, X. Vilajosana, and S. Pollin, "Improving reliability and scalability of LoRaWANs through lightweight scheduling," *IEEE Internet Things J.*, vol. 5, no. 3, pp. 1830–1842, Jun. 2018.

[31] J. Lee, W. Jeong, and B. Choi, "A scheduling algorithm for improving scalability of LoRaWAN," in *Proc. Int. Conf. Inf. Commun. Technol. Convergence*, 2018, pp. 1383–1388.

[32] A. Triantafyllou, P. Sarigiannidis, T. Lagkas, I. D. Moscholios, and A. Sarigiannidis, "Leveraging fairness in LoRaWAN: A novel scheduling scheme for collision avoidance," *Comput. Netw.*, vol. 186, 2021, Art. no. 107735.

[33] R. Hamdi, M. Qaraqe, and S. Althunibat, "Dynamic spreading factor assignment in LoRa wireless networks," in *Proc. IEEE Int. Conf. Commun.*, 2020, pp. 1–5.

[34] H. Fawaz, K. Khawam, S. Lahoud, S. Martin, and M. El Helou, "Cooperation for spreading factor assignment in a multi-operator LoRaWAN deployment," *IEEE Internet Things J.,* vol. 8, no. 7, pp. 5544–5557, Apr. 2020.

[35] T. Yatagan and S. Oktug, "Smart spreading factor assignment for LoRaWANs," in *Proc. IEEE Symp. Comput. Commun.*, 2019, pp. 1–7.

[36] V. Hauser and T. Hégr, "Proposal of adaptive data rate algorithm for LoRaWAN-based infrastructure," in *Proc. IEEE 5th Int. Conf. Future Internet Things Cloud*, 2017, pp. 85–90.

[37] M. Slabicki, G. Premsankar, and M. Di Francesco, "Adaptive configuration of LoRa networks for dense IoT deployments," in *Proc. IEEE/IFIP Netw. Oper. Manage. Symp.*, 2018, pp. 1–9.

[38] R. Marini, W. Cerroni, and C. Buratti, "A novel collision-aware adaptive data rate algorithm for LoRaWAN networks," *IEEE Internet Things J.*, vol. 8, no. 4, pp. 2670–2680, Feb. 2021.

[39] N. Sornin and L. Champion, "Signal concentrator device," U.S. Patent 9794095, Oct. 17, 2017.

[40] L. Alliance, "LoRaWAN specification v1.0.3, 2018," LoRa Alliance, pp. 1–82, 2015. [Online]. Available: https://lora-alliance.org/sites/default/files/2018-07/lorawan1.0.3.pdf

[41] E. R. Committee "ERC Recommendation 70–03: Relating to the use of Short Range Devices (SRD)," Sep. 2015.

[42] J. Lyu, D. Yu, and L. Fu, "Achieving max-min throughput in LoRa networks," in *Proc. Int. Conf. Comput., Netw., Commun.*, 2020, pp. 471–476.

[43] D. Stoyan, W. Kendall, and J. Mecke, *Stochastic Geometry and Its Applications (Wiley Series in Probability and Mathematical Statistics: Applied Probability and Statistics)*. Hoboken, NJ, USA: Wiley, 1987.

[44] M. Haenggi, *Stochastic Geometry for Wireless Networks*. Cambridge, U.K.: Cambridge Univ. Press, 2012.

[45] Semtech, SX1272/3/6/7/8, "LoRa Modem Design Guide AN1200. 13," Revision 1, Jul. 2013.

[46] M. Anjum, M. A. Khan, S. A. Hassan, A. Mahmood, H. K. Qureshi, and M. Gidlund, "RSSI fingerprinting-based localization using machine learning in LoRa networks," *IEEE Internet Things Mag.*, vol. 3, no. 4, pp. 53–59, Dec. 2020.

[47] K. Lam, C. Cheung, and W. Lee, "RSSI-based LoRa localization systems for large-scale indoor and outdoor environments," *IEEE Trans. Veh. Technol.*, vol. 68, no. 12, pp. 11778–11791, Dec. 2019.

[48] M. Anjum, M. A. Khan, S. Ali Hassan, A. Mahmood, and M. Gidlund, "Analysis of RSSI fingerprinting in LoRa networks," in *Proc. 15th Int. Wireless Commun. Mobile Comput. Conf.*, 2019, pp. 1178–1183.

[49] T. Wattananavin, K. Sengchuai, N. Jindapetch, and A. Booranawong, "A comparative study of RSSI-based localization methods: RSSI variation caused by human presence and movement," *Sens. Imag.*, vol. 21, no. 1, pp. 1–20, 2020.